Analytica Chimica Acta 1156 (2021) 338360

Contents lists available at ScienceDirect

Analytica Chimica Acta

journal homepage: www.elsevier.com/locate/aca

Ultrasensitive and easily reproducible biosensor based on novel doped MoS_2 nanowires field-effect transistor in label-free approach for detection of hepatitis B virus in blood serum

Mohsen Shariati [a], Maryam Vaezjalali [b], Mahdi Sadeghi [a, *]

[a] Medical Physics Department, School of Medicine, Iran University of Medical Sciences, P.O. Box 14155-6183, Tehran, Iran
[b] Department of Microbiology, School of Medicine, Shahid Beheshti University of Medical Sciences, P.O. Box 19839-63113, Tehran, Iran

HIGHLIGHTS

- HBV DNA FET biosensor in label free and easily reproducible setup was fabricated.
- Biosensor was materialized by novel ZnO (NPs) doped MoS_2 NWs through VLS technique.
- Device showed sensitivity at 1 fM LOD with response time of 25 s with 96% stability.
- Device diagnosed DNA targets in a linear concentration range from 0.5 pM to 50 μM.
- FET device showed the high specificity by discriminating two different human samples.

GRAPHICAL ABSTRACT

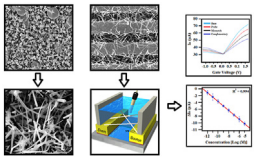

ARTICLE INFO

Article history:
Received 18 November 2020
Received in revised form
23 February 2021
Accepted 24 February 2021
Available online 6 March 2021

Keywords:
Biosensor
Hepatitis B Virus
MoS_2 nanowires
Field-effect transistor
Label-free mechanism

ABSTRACT

An ultrasensitive field-effect transistor (FET) for hepatitis B virus deoxyribonucleic acid (HBV DNA) detection in label free approach and easily reproducible setup was reported. The fabricated FET biosensor was materialized by ZnO doped MoS_2 nanowires (NWs). This report introduced a novel structure of the MoS_2 in bio-sensing approach. Because of unique electrical and structural properties of MoS_2, HBV biosensor could demonstrate the high sensitivity and showed the detection limit of 1 fM. The MoS_2 NWs fabrication was materialized through ZnO based vapor-liquid-solid (VLS) technique. The fabricated device could measure the DNA targets in a linear concentration range from 0.5 pM to 50 μM. The dynamic response time of FET biosensor was 25 s. The functionality of the NWs biosensor for label-free measurements could be repeated for several times without any significant malfunction and biosensor could retain 96% of its initial response after eight weeks maintenance. The HBV biosensor showed high selectivity by discrimination the complementary DNA oligonucleotides from non-complementary and the mismatch (1, 2 and 3 bases) oligonucleotides. The materialized platform was desirably reproduced for HBV concentrations in human serum. The specificity of the biosensor was evaluated against several different types of DNAs and the fabricated device showed the outstanding performance. In order to optimize the device functionality, the biosensor was checked for two different human samples and device could distinguish the samples from each other in the same manner.

* Corresponding author.
E-mail address: sadeghi.m@iums.ac.ir (M. Sadeghi).

https://doi.org/10.1016/j.aca.2021.338360
0003-2670/

1. Introduction

Hepatitis B virus is the main cause of hepatocellular carcinoma, liver cirrhosis and finally the death of more than a million people a year [1–5]. The range of clinical symptoms of this infection varies and leads to acute, chronic infection, without clinical symptoms and even rapid infection [6]. Acute infection is relatively self-limiting and is associated with inflammation and necrosis of hepatocytes. Mortality from acute infection is about 0.5–1% [7]. The presence of HbsAg in the blood or serum for more than six months indicates a chronic infection [8]. Age is a key factor in determining the risk of a chronic infection development, so that the risk of chronic infection in infants born to HBeAg-positive mothers is about 90% positive and for children under five is 20–60%, and the probability of chronic infection development in adults is about less than 5%. In people with chronic infections, the range of disease varies from person to person [9]. In some people, the infection is inactive and does not lead to severe liver disease, but in others it leads to fibrosis, cirrhosis, and enhancement of the hepatocellular carcinoma risk, which can occur years after the initial infection [10]. Long-term studies in untreated people with chronic infections have shown that the risk of spreading the infection to cirrhosis five years after the onset of the infection is about eight to 20%. Consequently, the accurate detection of this specific virus is tremendously important in the diagnosis of pathogenic and genetic diseases [11].

Recently, nanomaterial-based bio-sensing strategies have enabled substantial developments in the HBV detection [12]. Among the functional and advanced materials, MoS_2-based materials in nano and micro scale have been used specifically for biosensors and DNA aptamer [13–18]. A new nanoenzyme was introduced to a label-free electrochemical immunosensor for HBsAg detection [19]. The PtPd NCs@MoS_2 was used for sensitive detection of HBsAg, which was ascribed to their superior peroxidase activity, good conductivity and high specific surface area and synergistic amplification for current signals [19]. Compared with the detection limit of colorimetric method; 3.3 pg/mL, the electrochemical technique shows a lower detection limit; 10.2 fg/mL, and a wider linear range from 32 fg/mL to 100 ng/mL [19]. A highly selective and sensitive aptamer-based “capture-release” fluorescence detection of a malarial biomarker, i.e., Plasmodium lactose dehydrogenase (pLDH) protein, using single-layer two-dimensional MoS_2 nanosheets was demonstrated [20]. The detection of the target pLDH protein utilizing the aptamer-nanosheet sensing platform was rapid and could be easily completed within 10 min [20]. An ultrasensitive sandwich-type electrochemical immunosensor was proposed for quantitative detection of hepatitis B surface antigen [21]. First, the porous graphene oxide/Au composites with good conductive ability were employed to accelerate the electron transfer on the electrode interface [21]. Furthermore, the amino functionalized molybdenum disulfide @ cuprous oxide hybrid with coral morphology was prepared to combine platinum nanoparticles for achieving signal amplification strategy [21]. Under optimal conditions, a linear relationship between current signal and hepatitis B surface antigen concentration in the broad range from 0.5 pg/mL to 200 ng/mL, with detection limit of 0.15 pg/mL (signal-to-noise ratio of 3) was obtained [21]. MoS_2 nanosheets were applied to detect the HBV analyte. The fluorescence of polymer-capped Ag nanoclusters was quenched by MoS_2 nanosheets [22]. Addition of ssDNA to the MoS_2 nanosheets, prevent the MoS_2 nanosheets from aggregation and blocked the fluorescence from being restored [22]. If complementary sequences was added, a dsDNA will be formed that does no longer prevent aggregation and fluorescence is restored [22].

In this regard, a new platform for detecting HBV DNA based on ZnO doped MoS_2 NWs FET electrode was materialized. The biosensing measurements were performed by FET (voltage-current under gating control) mechanism. The HBV DNA probe was immobilized on the ZnO doped MoS_2 NWs and hybridization of the complementary DNA target was detected. The ZnO doped MoS_2 NWs biosensor could excellently distinguish the complementary DNA target from other targets. The ZnO doped MoS_2 NWs biosensor showed the detection of the HBV DNA in blood serum samples and indicated the interesting results in the practical applications. The stability and specificity of the fabricated biosensor were investigated and device showed interesting result. The easily reproducible capability of this approach would open windows for materialization of the pilot diagnosis in HBV detection.

2. Experimental details

2.1. Chemicals and materials

The precursors in high purity including molybdenum, zinc metals and sulfur were purchased from Merck Co. (Germany). The silicon wafers (Si; p-type [100]) as substrate were prepared from CGS Co. (Iran). The K3Fe(CN)6/K4Fe(CN)6 (1 mM) aqueous solution as electrolyte was use to EIS measurements for evaluating gate performance. The selected oligonucleotides were prepared under dictated protocol by Bioneer Co. (South Korea). The 25-mer sequences including; probe (ssDNA), complementary, non-complimentary and mismatch targets were evaluated with basic local alignment search tool. The oligonucleotides were washed by SD water and kept at −30 °C temperature in the freezer. The DNA materials are defined as followed:

The sequences of DNA oligonucleotides.

Sequence name	Sequence of oligonucleotides	Company (Country)
Probe	5′-AAT GTG CTC CCC CAA CTC CTC-3′	Bioneer Co.
Target	5′-GAG GAG TTG GGG GAG CAC ATT-3′	Bioneer Co.
One-point Mismatch	5′-GAG GAG TTG GGG GAG CTC ATT-3′	Bioneer Co.
Two-point Mismatch	5′-GAC GAG TTG GGG GAG CTC ATT-3′	Bioneer Co.
Three-point Mismatch	5′-GAC GAG TTG CGG GAG CTC ATT-3′	Bioneer Co.
Non-complementary	5′-AAA AGG TGT AAG CGT TTG CCG-3′	Bioneer Co.

2.2. Fabrication of the doped MoS_2 NWs

For fabrication of the ZnO doped MoS_2 NWs, the silicon (Si P-type) substrates were used to grow NWs. The substrates were cleansed in ethanol bath and ultrasonically washed in acetone. The preparation steps were conducted in 20 min. The substrates were eventually immersed in de-ionized water for 1 h and dried in argon gas. The ZnO doped MoS_2 NWs were fabricated in physical vapor deposition (PVD) mechanism. The ZnO doped MoS_2 NWs were synthesized by magnetron RF sputtering in 13.56 MHz frequency followed by annealing and thermal evaporation. The sputtering process was conducted in 7×10^{-7} mbar pressure and temperature at 100 °C. The sputtering target was ZnO disc in 99.999% purity. The deposition conditions after argon gas introduction were kept at flow rate in 35 sccm, power in 100 W and temperature at 100 °C. The chamber working pressure was 8×10^{-2} mbar in 25 sccm rate. The ZnO thin film thickness was monitored with a crystal thickness monitor up to 900 nm. Then the ZnO films were heat treated in annealing process. After growth of short ZnO nanoparticles (NPs), the process for MoS_2 NWs fabrication was gotten started. After the ZnO NPs materialization, they were put in tubular furnace as support layer. The molybdenum and sulfur source were put in boat at 99.999% purity (20:1). The heat treatment process was conducted at 1600 °C temperature with argon and oxygen (Ar:O_2 ratio 20:1) presence for 90 min it is important to note, until 1000 °C; no oxygen introduction was conducted. The oxidation step was performed under vacuum condition. Finally the doped MoS_2 NWs films were positioned in argon gas for NWs materialization. The final outcome was the white thin film with a large number of the doped MoS_2 NWs.

2.3. Fabrication of NWs FET biosensor device

To materialize ZnO based MoS_2 NWs FET biosensor, the fabricated NWs on Si substrates were sonicated in ethanol bath for 1 h, and then the suspension was drop-casted onto the FET electrode. The FET electrode was comprised by a highly doped Si (p-type) with a SiO_2 thin film (100 nm). The SiO_2 thin layer was served as back gate terminal. The back gate electrode was used to modulate the charged carriers and their density. The source and drain electrodes (Ti/Au (20/60 nm) were fabricated through electron beam lithography (EBL) with spacing of 2 μm. Prior to the source and drain electrodes defining, the Ti thin film was passivated by sputtering. The FET device was cleansed in ethanol followed by lift-off process.

2.4. Preparation of ssDNA probe modified electrode and hybridization process

In order to conduct the FET measurements for NWs electrode; first the NWs electrode surface was prepared in clean room for hindering from bacterial contamination. Then the ss-DNA samples (5 μL; in different concentration) which sonicated in Nafion solution (5 wt %, 10 μL) for 10 min were drop-casted on the electrode surface. In order to remove the non-immobilized ssDNA oligonucleotides; the probe ssDNA modified NWs electrode was dried under argon gas presence at room temperature for 2 h and then gently cleansed with Britton–Robinson (BR) buffer. For performing the hybridization process, the probe electrode was washed with Milli-pore water and rinsed with buffer solution. A hybridized buffer solution was used to hybridize the probe with target. The hybridized buffer solution was 0.5 mM sodium chloride and 0.05 mM sodium citrate. The hybridization process was conducted by drop-casting of the hybridized buffer solution (5 μL) containing target DNA (different concentrations of complementary, non-complementary and mismatches) on the probe modified electrode at room temperature and preserved for 30 min. Then, the NWs/ssDNA/target DNA electrode was washed with BR buffer solution to remove the non-hybridized dsDNA and the FET measurements were implemented.

2.5. Instrumental characterizations and electronic measurements

The morphology measurements and characterization investigations were conducted by a scanning electron microscopy (Hitachi S-4160, Japan) and a transmission electron microscopy (Philips, CM-30). The crystallographic measurements were conducted by a Rigaku D/max RB X-ray diffractometer, XRD-6000, Japan, with *CuKα* line (40 kV, 100 mA). The electrical transport parameters were conducted and measured by a semiconductor parameter analyzer (HP−4155C).

3. Results and discussion

3.1. Morphological and crystal structure characterizations

The morphological and crystal structure characterizations of the fabricated doped MoS_2 NWs were investigated by FESEM and HRTEM microscopic measurements. Fig. 1 (A) shows the process before MoS_2 NWs growth. The ZnO NPs shape and their accommodations for MoS_2 growth were clear. The ZnO NPs could bring the key parameters for NWs growth. As it is seen in Fig. 1A, the NWs could germinate from ZnO NPs. Fig. 1B shows the materialized MoS_2 NWs morphology. Fig. 1B shows the MoS_2 NWs in wire-like shape and they are around 50 nm in wide and several microns in length. The surface of the supporting layer is uniformed with a large number of the MoS_2 NWs. Fig. 1C shows the TEM and HRTEM images of a doped MoS_2 NW with wire like morphological structure. The bright-field TEM image of doped MoS_2 NW shows the well-defined stretched structure. The TEM image shows that the MoS_2 NW is grown by the self-assembly (surface layer by layer) VLS approach and possesses perfect sharp edges and well-defined facets with the uniform size of 50 nm. The HRTEM image (Fig. 1C, inset) shows the spacing facets of the MoS_2 NW correspond to (002) plane with the lattice inter-plane spacing of 0.72 nm. The HRTEM image validates the MoS_2 phase structure [20]. Fig. S1 shows the XRD pattern of the doped MoS_2 NWs phase structure. Fig. S1 shows the compatibility and accordance between HRTEM and XRD pattern results.

Fig. 1D shows the electrode setup in schematic image. The A sign is related to the electrode (drain vs. source) spacing distance. Fig. 1E shows FESEM image of NWs FET device. Fig. 1E shows the random distribution of MoS_2 NWs on the FET device surface. Fig. 1F shows the schematic picture of the fabricated HBV biosensor setup based on the NWs-FET device. The reference electrode as gate electrode was positioned on top of the sensing system.

3.2. NWs-FET device characteristics and sensing mechanism

The device electronic transfer measurements were curved in Fig. 2A. Fig. 2A shows the I_{ds} vs. V_G for bare electrode, probe, mismatch and complementary targets at 1 μM concentration. Fig. 2A exhibits ambipolar field effect properties of the bio-sensing device. The FET biosensor was biased via V_G in different values varying from −1.25 to 1.75 V in fixed V_{ds} at 0.1 V. The charge neutrality point voltage (V_{cnp}) was measured at the minimum conductance point of the transfer curve also known as the Dirac point. The transfer curve of the biosensor was shifted to the positive values after modifying with probe oligonucleotides. The positively shift by addition of mismatches and complementary HBV DNA sequence (aptamer) was consistently repeated in Fig. 2A. The

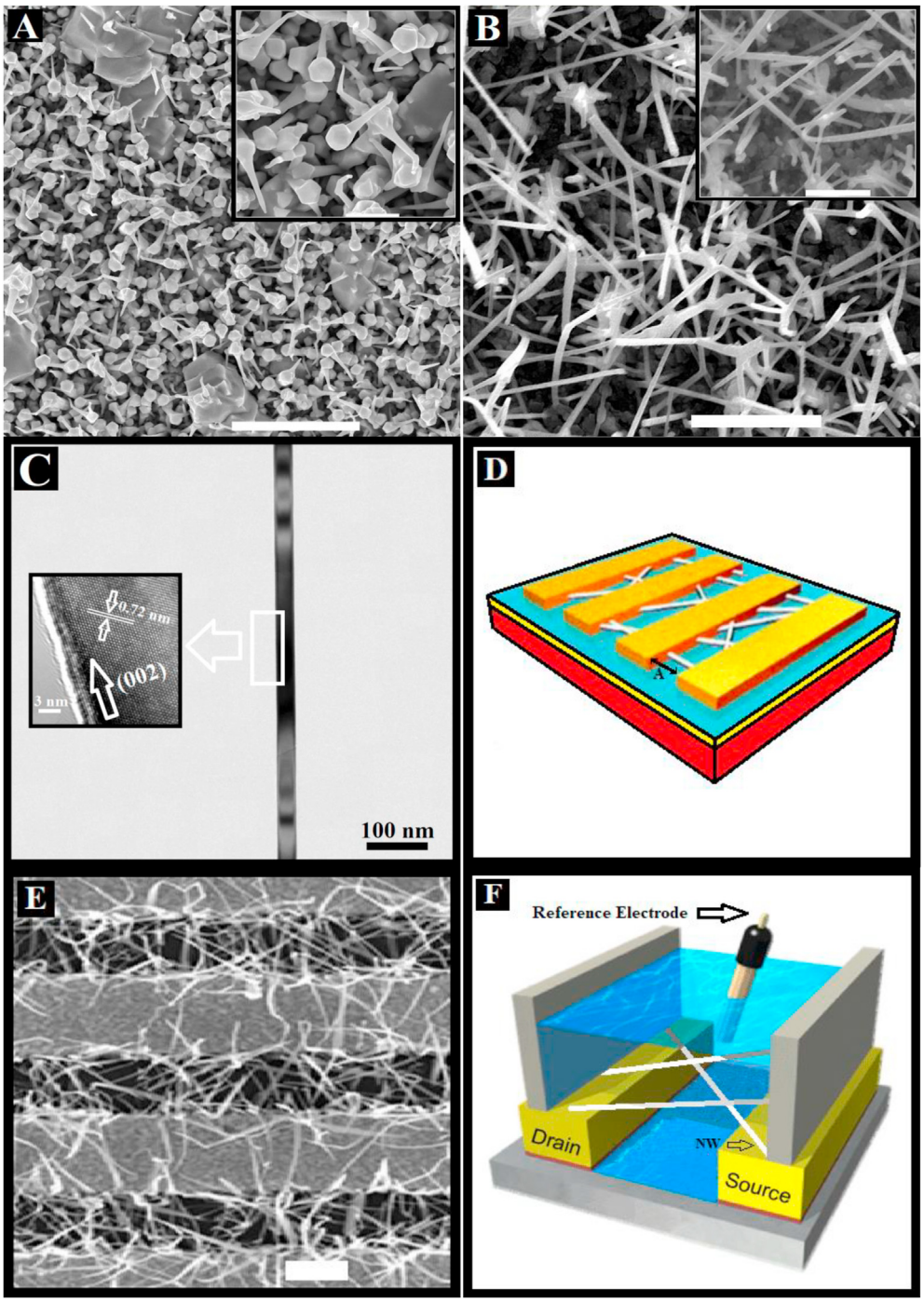

Fig. 1. The morphological and crystal structure characterizations of the fabricated doped MoS_2 NWs and biosensor setup. (A) The germination from ZnO NPs for NWs growth, Scale: 2 μm, (inset Scale: 500 nm). (B) The materialized MoS_2 NWs. The MoS_2 NWs in wire-like shape and around 50 nm in wide, Scale: 2 μm, (inset Scale: 500 nm). (C) The TEM and HRTEM images of the doped MoS_2 NW with wire like morphological structure. (D) The electrode setup in schematic image. The A sign is related to the electrode (drain vs. source) spacing distance 2 μm. (E) The FESEM image of NWs FET device, scale: 2 μm. (F) The schematic picture of the fabricated HBV biosensor setup based on the NWs-FET device.

negative electrostatic gating and the electrostatic and steric repulsion associated with charge exchange between sulfur and negative charges of DNA sequences induced the positive direction shift of V_{cnp} in The transfer curve [23]. The negative electrostatic gating effect was intensively induced to introduce the excess hole-based carriers to the surface and conduct the positive shift of the V_{cnp}. The X-ray photoelectron spectroscopy (XPS) was conducted to further investigate the oligonucleotides attachment on the NWs surface. The immobilization bond and interaction between the virus DNA and MoS_2 nanowires was mainly due to coordinate covalent bonds. The chemical coordinate bond was formed due to the donation of a lone electron pair by active and non-binding sulfur atom to oxygen atom. Fig. S2 shows the XPS spectra of NWs samples for ds-complementary, mismatch, non-complementary targets and ss-probe. As it can be seen in the XPS measurements for the NWs sample, noticeable N 1s peak intensity changes were observed at the N 1s peak, because of the attachment/interaction of ssDNA with the surface of NWs [23–26]. In addition, N 1s (400.1 eV)

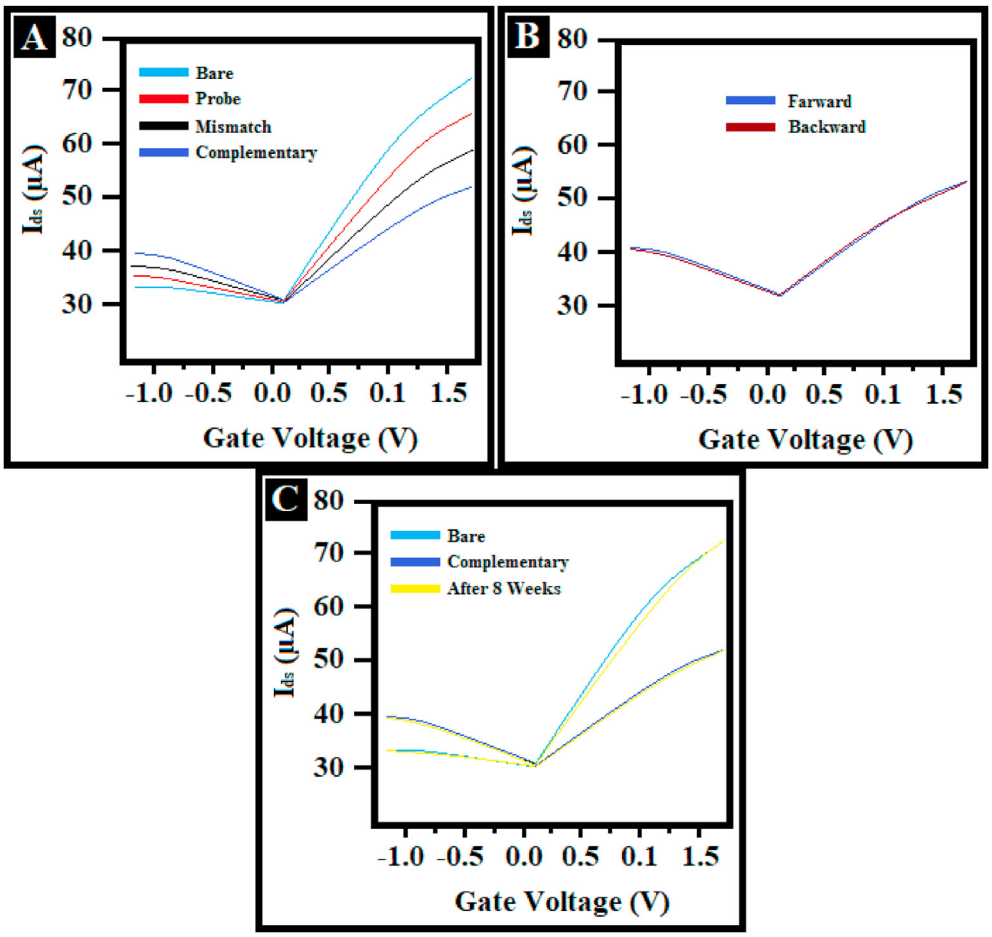

Fig. 2. (a) Transfer characteristics of the doped MoS_2 NWs-FET for the bare FET and after immobilization of 1 μM probe oligonucletides, mismatches sequence and complementary target. (b) Transfer characteristics of the doped MoS_2 NWs-FET with forward V_G (blue) and backward V_G (dark brown). (C) The stability measurements of the biosensor for probe and target investigation after 8 weeks maintenance (yellow line). (For interpretation of the references to color in this figure legend, the reader is referred to the Web version of this article.)

belongs to the amino functionalities in the ssDNA which obviously validates the attachment of ssDNA on the NWs surface (part A). The core-level C 1s XPS spectra of the NWs-ssDNA sample showed four main peaks; the main peak at 282.9 eV in the C 1s spectrum corresponds to carbon species in the ssDNA bonded to NWs crystal lattice, whereas other peaks located at 289.5, 288.1 and 286.7 eV can be ascribed to the adsorbed oxygen species which tangled on the NWs-ssDNA surface (part B) [23–26]. The core-level O 1s XPS spectra of the NWs-ssDNA sample showed two peaks; the main peak at 531.1 eV in the O 1s spectrum corresponds to oxygen agents in the NWs-ssDNA sample crystal lattice, whereas the peak located at 532.7 eV can be ascribed to the adsorbed oxygen species on the NWs-ssDNA sample (part C) [23–26]. The P 2p XPS spectrum shows the phosphorus attachment on the NWs-ssDNA sample crystal lattice surface (part D). The core-level S 2p XPS spectra of the NWs-ssDNA sample showed two peaks; the main peak with the S $2p_{3/2}$ binding energy at 162.2 eV in the S 2p spectrum corresponds to sulfur agents swapped with non-bridging oxygen atom in the NWs-ssDNA sample crystal lattice, whereas the peak located at 163.4 eV can be ascribed to the sulfur-coordination site electrostatically adsorbed on the neighboring DNA phosphate linkage in the NWs-ssDNA sample (part E) [23–26].

In order to evaluate the stability and reproducibility of doped MoS_2 NWs FET, the transfer curve was tested in forward and backward gate-source voltage in successive sweeps (Fig. 2B). The fabricated doped MoS_2 NWs FET device showed the stability by exhibiting the forward (blue) and backward (dark brown) gate-source voltage sweeps overlap (Fig. 2B).

The oligonucleotides bond to the surface and their immobilization to the NWs surface mainly were due to thiol-based bond. By injection of the HBV DNA solution to the NWs surface, the negatively charged phosphate-backbone made the thiol-based bond materialization. The thiol-based bond was originated from sulfur agents that swapped with non-bridging oxygen atom in the NWs-ssDNA sample crystal lattice, and bond ascribed to the sulfur-coordination site electrostatically adsorbed on the neighboring DNA phosphate linkage in the NWs-ssDNA sample (see Fig. S2). Fig. 2C shows the stability measurements of the biosensor for probe and target investigation after 8 weeks maintenance. Fig. 2C shows the after 8 weeks (yellow line) preservation in freezer and the biosensor could retain 96% of its initial response after eight weeks maintenance.

3.3. Real-time responses of doped MoS_2 NWs-FET biosensor

In order to investigate the dynamic response of the doped MoS_2 NWs-FET biosensor, the titrations of HBV DNA were measured by observing the I_{ds} as a function of time. Fig. 3 shows the dynamic properties of the doped MoS_2 NWs-FET biosensor as a function of time at different analyte (complementary target) concentrations.

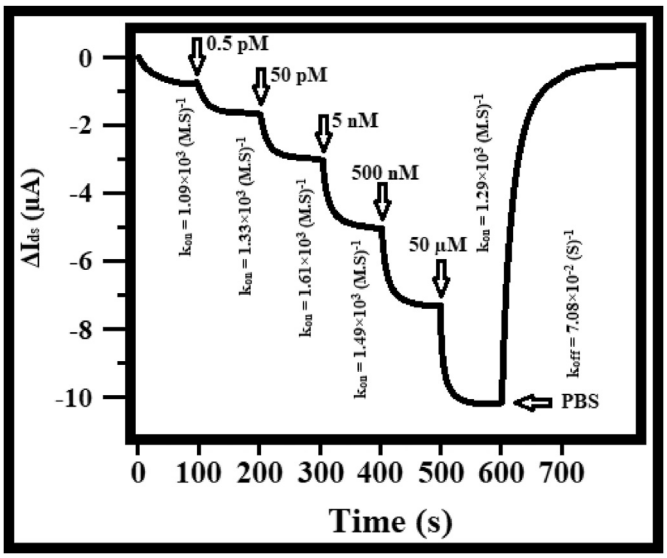

Fig. 3. The real-time response of the doped MoS_2 NWs-FET at different concentrations injected progressively from 0.5 pM to 50 µM.

Fig. 3 showed that the dynamic response time of the DNA biosensor was 25 s. As the analyte (complementary target) concentration was enhanced, the I_{ds} values were decreased. The DNA biosensor responded instantaneously to the concentration enhancement for several minutes, Fig. 3. In order to calculate the kinetic constant, the Langmuir formulation was applied. It has been known that the biosensor response to current changes due to immobilization of the oligonucleotides on the doped MoS_2 NWs-FET and device surface coverage was linear.

The channel current thus is described as absorption Eq. (1) and desorption Eq. (2) [23]:

$$\Delta I_{ds} = \Delta I_{max}\left(1 - e^{-(k_{on}[A]+k_{off})t}\right) \quad (1)$$

and

$$\Delta I_{ds} = \Delta I_{max}\left(e^{-k_{off}t}\right) + I_r \quad (2)$$

Where, ΔI_{ds} indicates drain-source current change at oligonucleotides immobilization time, t is the equilibrium setting time of the applied concentration and ΔI_{max} indicates the maximum response signal at HBV DNA concentration [23]. The association and dissociation rate constant are indicated by k_{on} and k_{off}, respectively. The I_r indicates the amount of immobilized oligonucleotides which deposed after HBV DNA desorption. In order to calculate the k_{on}, the binding constants were measured independently for each of the HBV DNA concentrations. The dissociation rate constant was calculated by fitting the dissociation phase. The K_D (binding equilibrium constant) in range from 4.23×10^{-5} to 4.98×10^{-5} M was calculated by the ratio of the association (binding) constant and dissociation (nonbinding) rate constant. The biosensor showed the limit of detection (LOD) of 1 fM. This very low LOD shows the outstanding capability of the fabricated biosensor. The measurement of LOD parameter was calculated by $Y = S_b + 3\sigma_b$, which σ_b and S_b are the standard deviation and the signal of the blank, respectively. The $3\sigma_b$ was the standard deviation value from the 20 blank tests.

3.4. Selectivity, sensitivity, and regeneration of the HBV DNA sensor

The sensitivity properties of the doped MoS_2 NWs-FET biosensor by successively injecting different oligonucleotides concentrations into the device surface have been investigated (Fig. 4A). The sensitivity measurements were conducted in concentration range from 0.5 pM to 50 µM. The repeatability of the biosensor in 3 samples for each concentration was performed in five tests.

The drain-current parameter by HBV DNA concentration enhancement was decreased. At n-type region, in fact at $V_{gs} = 1.25$ V, the transfer curve shows linear treatment. Fig. 4B shows the calibration curve for drain-current changes vs. HBV DNA concentration. The calibration curve shows a good linear relationship between drain-current changes and oligonucleotides concentration (in logarithm scale) for concentration range from 1 pM to 10 µM. Fig. 4B shows the high sensitivity for proposed biosensor in comparison previous works, see Table 1. Table 1 compares this work quantitatively with conducted researches that have been reported for detecting HBV DNA [9,23–36]. As shown in Table 1, the LOD of the doped MoS_2 NWs-FET biosensor is one or several orders lower than most of the reported results. The high sensitivity of the sensor can be attributed to the high surface to volume ratio and large specific surface area of MoS_2 NWs (Fig. 2C). Due to the high surface to volume ratio of the doped MoS_2 NWs, the bond sites were comprehensively enhanced. This made the adsorption sites very attractive for HBV DNA oligonucleotides immobilization. The selectivity of the fabricated HBV DNA biosensor was evaluated by exposing the doped MoS_2 NWs-FET to four types of target sequences, including single base-mismatch, two base-mismatch, three base-mismatch DNA, complementary DNA. Fig. 4C shows the selectivity of the probe, one base-mismatch, two base-mismatch and three base-mismatch DNA and complementary targets. Compared to the complementary DNA sequence (Fig. 4C), the drain-source changes of two and three base-mismatch DNA oligonucleotides were gradually decreased due to low or non-specific hybridization on ssDNA probe on doped MoS_2 NWs. The materialized HBV DNA biosensor could highly discriminate the complementary DNA from mismatched DNA targets and show the significant selectivity. In order to regenerate the doped MoS_2 NWs-FET biosensor for reusing in the successive bio-sensing measurements, 2 M NaCl applied to the bio-sensing system. The regeneration process was conducted by oligonucleotides decomposition. In other means, the HBV DNA should be split from probe aptamer. Fig. 4D shows the reuse of biosensor after regeneration process. The high salt concentrations usage helped HBV DNA release from the HBV DNA probe aptamer. The investigation was performed after several times without any failure and malfunction.

3.5. HBV DNA analysis in real sample

In order to investigate the capabilities of the fabricated biosensor to sense the complex biological matrix, the doped MoS_2-FET biosensor was used to test the human serum samples.

Fig. 5A shows the transfer curves of the doped MoS_2-FET biosensor in different concentrations, ranging from 0.5 pM, 50 pM, 5 nM, 50 nM and 0.5 µM. For human samples sensing, the solutions were loaded with 10% diluted human serum. The proposed biosensor exhibited the sensing treatment for human samples similar to those prepared in buffer. The drain-source current was decreased as the concentration was enhanced see Fig. 5A. The calibration curve shows a linear treat for relationship between drain-source current changes and concentration (logarithmic scale), Fig. 5B. In order to evaluate the specificity of the fabricated biosensor, the HBV DNA assay was investigated in different human sample. Fig. 5C shows the results of the transfer curves for several concentrations for second human sample. The second sample was

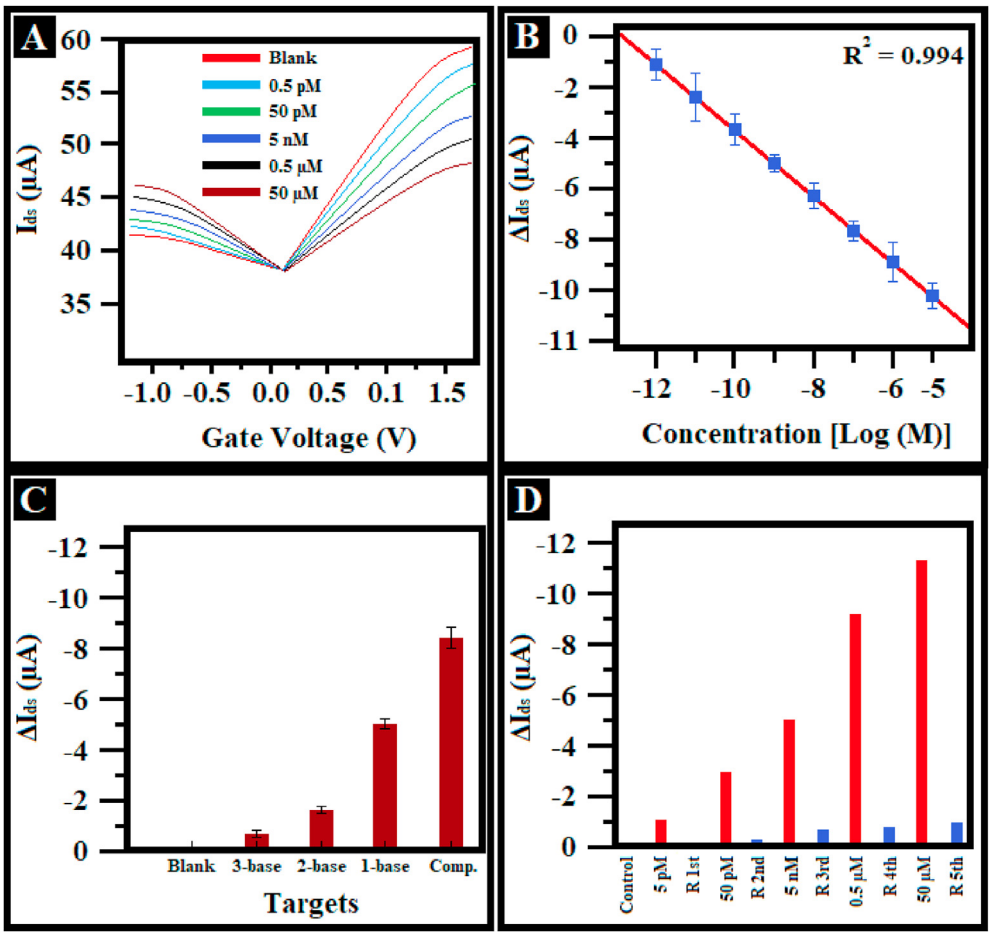

Fig. 4. (A) The sensitivity responses of the HBV doped MoS_2 NWs-FET biosensor. (A) The calibration plot for doped MoS_2 NWs-FET biosensor. The drain-source current changes against concentration (logarithmic scale, 1 pM to 10 μM, $R^2 = 0.994$. (C) The specificity measurements for mismatches (1, 2 and 3-bases) oligonucleotides samples in comparison to complementary target. (D) The regeneration measurements for testing the repeatability of the biosensor.

conducted after applying the Laser and X-ray radiation associated with putting in shrimp alkaline phosphatase (SAP) and washing the device in the much purified DIW. The transfer plots of the second sample also showed a similar behavior to the first sample, Fig. 5C. Fig. 5D shows the device behavior by studying the drain-source changes for second sample in different samples. Finally the device was cleansed in Laser and X-ray radiation followed on washing by DIW. The obtained results demonstrate that the materialized device based on the doped MoS_2 NWs-FET biosensor is available for HBV DNA diagnosis in real biological samples.

Table 1
The comparison among the reported biosensors.

Sensing Technique	Concentration range	LOD	REF.
EIS-Laser	**0.1 pM to 10 μM**	**1 fM**	[9]
EIS-(In + Au) NCs	**0.1 pM to 0.1 μM**	**0.1 fM**	[23]
G-FET	**0.5 pM–50 μM**	**0.5 pM**	[27]
EIS	**0.1–20 nM**	**34 pM**	[28]
EIS	**13.6 nM–10μM**	**13.6 nM**	[29]
LSPR	**10 pM–10 μM**	**10 pM**	[30]
LSPR	**0.01–100 μM**	**10 nM**	[31]
Fluorometric	**3–320 μM**	**0.45 nM**	[32]
Fluorometric	**140 nM–17.5 mM**	**140 nM**	[33]
Fluorometric	**0.1–1 mM**	**24 μM**	[34]
Fluorometric	**10–4000 pM**	**4.8 pM**	[35]
G-FET	**400 nM–50μM**	**400 nM**	[36]
This work	**0.5 pM to 50 μM**	**1 fM**	**This Work**

4. Conclusions

In this report, an ultrasensitive and easily reproducible biosensor based on doped MoS_2 NWs FET in label-free approach for detection of HBV DNA in blood serum has been fabricated. The novel doped MoS_2 NWs were materialized through ZnO based VLS technique. The HBV biosensor could detect the small molecules at LOD of 1 fM in a linear concentration range from 0.5 pM to 50 μM. The fabricated biosensor showed good repeatability and stability and the materialized biosensor could retain 96% of its initial response after eight weeks maintenance. The proposed device showed high selectivity by discrimination the complementary sequences from the mismatch (1, 2 and 3 bases) sequences. The specificity of the biosensor was evaluated against several different types DNAs and it showed the outstanding performance. The proposed biosensor was fabricated in cost-free and reproducible process and could distinguish the human samples from each other.

CRediT authorship contribution statement

Mahdi Sadeghi: Conceptualization, Methodology, Software, Validation, Formal analysis, Investigation, Resources, Data curation, Writing – original draft, Visualization, Funding acquisition, Project administration, Visualization.

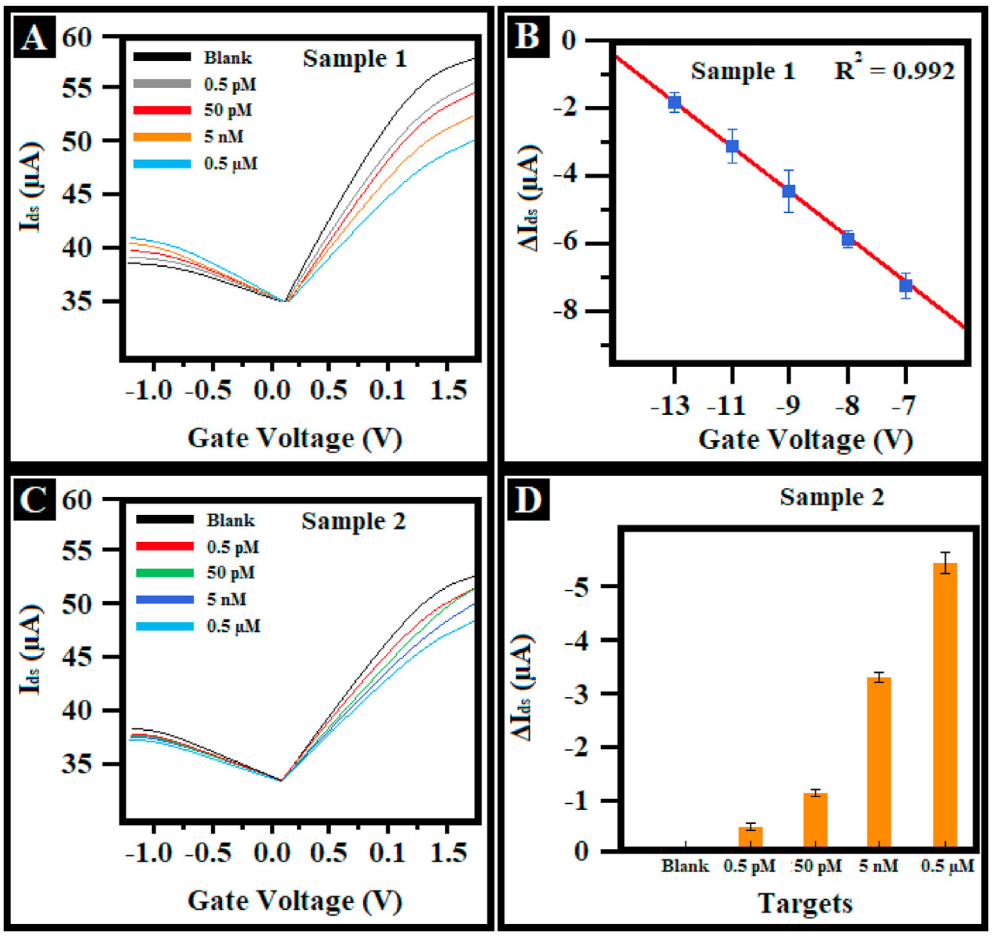

Fig. 5. (A) The sensitivity responses of the HBV doped MoS_2 NWs-FET biosensor for human serum, sample 1. (A) The calibration plot of the doped MoS_2 NWs-FET biosensor measurements for human serum, sample 1. The drain-source current changes against concentration (logarithmic scale, 0.1 pM to 0.1 µM, $R^2 = 0.992$. (C) The sensitivity responses of the HBV doped MoS_2 NWs-FET biosensor for human serum, sample 2. (D) The current responses of the doped MoS_2 NWs-FET for detecting HBV DNA in human serum, sample 2.

Declaration of competing interest

The authors declare that they have no known competing financial interests or personal relationships that could have appeared to influence the work reported in this paper.

Acknowledgments

The present article is financially supported by “Iran National Science Foundation: INSF” (Project Code: 98017074).

Appendix A. Supplementary data

Supplementary data to this article can be found online at https://doi.org/10.1016/j.aca.2021.338360.

References

[1] R. Riahi, K.E. Mach, R. Mohan, J.C. Liao, P.K. Wong, Molecular detection of bacterial pathogens using microparticle enhanced double-stranded DNA probes, Anal. Chem. 83 (2011) 6349–6354.
[2] C. Yang, M.E. Denno, P.P. JillVenton, Recent trends in carbon nanomaterial-based electrochemical sensors for biomolecules: a review, Anal. Chim. Acta 887 (5) (2015) 17–37.
[3] B. Negahdari, M. Darvishi, A. Asghar Saeedi, Gold nanoparticles and hepatitis B virus, artificial cells, Nanomedicine, and Biotechnology 47 (2019) 469–474.
[4] H. Ju, H. Zhao, Electrochemical biosensors for DNA analysis, Front. Biosci. 10 (2005) 37–46.
[5] J.K. Wen, X.E. Zhang, Z. Cheng, H. Liu, Y.F. Zhou, Z.P. Zhang, J.H. Yang, J.Y. Deng, A visual DNA chip for simultaneous detection of Hepatitis B virus, Hepatitis C virus and human immunodeficiency virus type-1, Biosens. Bioelectron. 19 (2004) 685–692.
[6] A. Escosura-Muiz, M. Maltez-da Costa, C. Sanchez-Espinel, B. Diaaz-Freitas, J. Fernandez-Suarez, A.F. Gonzalez-Fernandez, A. Merkoasi, Gold nanoparticle-based electrochemical magneto immunosensor for rapid detection of anti-Hepatitis B virus antibodies in human serum, Biosens. Bioelectron. 26 (2009) 1710–1714.
[7] M. Shariati, The field effect transistor DNA biosensor based on ITO nanowires in label-free hepatitis B virus detecting compatible with CMOS technology, Biosens. Bioelectron. 105 (2018) 58–64.
[8] A. Erdem, K. Kerman, B. Meric, U.S. Akarca, M. Ozsoz, DNA electrochemical biosensor for the detection of short DNA sequences related to the Hepatitis B virus, Electroanalysis 11 (1999) 586–587.
[9] M. Shariati, M. Sadeghi, Ultrasensitive DNA biosensor for hepatitis B virus detection based on tin-doped WO3/In2O3 heterojunction nanowire photo-electrode under laser amplification, Anal. Bioanal. Chem. 412 (2020) 5367–5377.
[10] J. Labuda, A.M.O. Brett, G. Evtugyn, M. Fojta, M. Mascini, M. Ozsoz, I. Palchetti, E. Palecek, J. Wang, Electrochemical nucleic acid based biosensors: concepts, terms, and methodology (IUPAC Technical Report), Pure Appl. Chem. 82 (2010) 1116–1187.
[11] H.J. Parab, C. Jung, J.H. Lee, H.G. Park, A gold nanorod-based optical DNA biosensor for the diagnosis of pathogens, Biosens. Bioelectron. 26 (2010) 667–673.
[12] B. Negahdari, M. Darvishi, A.A. Saeedi, Gold nanoparticles and hepatitis B virus, Artif. Cells Nanomed. Biotechnol. 47 (1) (2019) 469–474.
[13] K. Kalantar-zadeh, J.Z. Ou, T. Daeneke, M.S. Strano, M. Pumera, S.L.(Gras, Two-dimensional transition metal dichalcogenides in biosystems, Adv. Funct. Mater. 25 (2015) 5086–5099.
[14] H. Kim, H. Kim, C. Ahn, A. Kulkarni, M. Jeon, G.Y. Yeom, M. Lee, T. Kim, In situ synthesis of MoS_2 on a polymer based gold electrode platform and its application in electrochemical biosensing, RSC Adv. 5 (2015) 10134–10138.
[15] S. Su, H. Sun, F. Xu, L. Yuwen, C. Fan, L. Wang, Direct electrochemistry of

glucose oxidase and a biosensor for glucose based on A glass carbon electrode modified with MoS2 nanosheets decorated with gold nanoparticles, Microchimica Acta 181 (2014) 1497–1503.
[16] C. Zhu, Z. Zeng, H. Li, F. Li, C. Fan, H. Zhang, Single-layer MoS_2-based nanoprobes for homogeneous detection of biomolecules, J. Am. Chem. Soc. 135 (2013) 5998–6001.
[17] Y. Huang, Y. Shi, H.Y. Yang, Y. Ai, A novel single-layered MoS_2 nanosheet based microfluidic biosensor for ultrasensitive detection of DNA, Nanoscale 7 (2015) 2245–2249.
[18] J. Huang, L. Ye, X. Gao, H. Li, J. Xu, Z. Li, Molybdenum disulfide-based amplified fluorescence DNA detection using hybridization chain reactions, J. Mater. Chem. 3 (2015) 2395–2401.
[19] Z. Tan, H. Dong, Q. Liu, H. Liu, P. Zhao, P. Wang, Y. Li, D. Zhang, Z. Zhao, Y. Dong, A label-free immunosensor based on PtPd NCs@MoS2 nanoenzymes for hepatitis B surface antigen detection, Biosens. Bioelectron. 142 (2019), 111556.
[20] Geldert A. Kenry, X. Zhang, H. Zhang, C.T. Lim, Highly sensitive and selective aptamer-based fluorescence detection of a malarial biomarker using single-layer MoS2 nanosheets, ACS Sens. 1 (11) (2016) 1315–1321.
[21] F. Li, Y. Li, J. Feng, Z. Gao, H. Lv, X. Ren, Q. Wei, Facile synthesis of MoS2@Cu2O-Pt nanohybrid as enzyme-mimetic label for the detection of the Hepatitis B surface antigen, Biosens. Bioelectron. 100 (2017) 512–518.
[22] F. Qu, Y. Liu, R. Kong, J. You, A versatile DNA detection scheme based on the quenching of fluorescent silver nanoclusters by MoS2 nanosheets: application to aptamer-based determination of hepatitis B virus and of dopamine, Microchimica Acta volume 184 (2017) 4417–4424.
[23] M. Shariati, Impedimetric biosensor for monitoring complementary DNA from hepatitis B virus based on gold nanocrystals, J. Electrochem. Soc. 168 (2021), 016512.
[24] H. Yu, J. Li, G. Liu, G. Zhao, Y. Wang, W. Hu, Z. Deng, G. Wu, J. Gan, Y. Zhao, X. He, DNA backbone interactions impact the sequence specificity of DNA sulfur-binding domains: revelations from structural analyses, Nucleic Acids Res. 48 (15) (2020) 8755–8766.
[25] Y. Yang, G. Xu, J. Liang, Y. He, L. Xiong, H. Li, D. Bartlett, Z. Deng, Z. Wang, X. Xiao, DNA backbone sulfur-modification expands microbial growth range under multiple stresses by its anti-oxidation function, Sci. Rep. 7 (2017) 3516.
[26] T. Wang, R. Zhu, J. Zhuo, Z. Zhu, Y. Shao, M. Li, Direct detection of DNA below ppb level based on thionin-functionalized layered MoS2 electrochemical sensors, Anal. Chem. 86 (2014) 12064–12069.
[27] X. Shicai, Z. Chao, J. Shouzhen, H. Guodong, L. Xiaoyue, Z. Yan, L. Hanping, J. Li, L. Zhenhua, W. Xiaoxin, L. Mingzhen, W. Jihua, Graphene foam field-effect transistor for ultra-sensitive label-free detection of ATP, Sensor. Actuator. B Chem. 284 (2019) 125–133.
[28] T. Bao, H. Shu, W. Wen, X. Zhang, S. Wang, A sensitive electrochemical aptasensor for ATP detection based on exonuclease III-assisted signal amplification strategy, Anal. Chim. Acta 862 (2015) 64–69.
[29] L. Feng, Z. Zhang, J. Ren, X. Qu, Functionalized graphene as sensitive electrochemical label in target-dependent linkage of split aptasensor for dual detection, Biosens. Bioelectron. 62 (2014) 52–58.
[30] J.H. Park, J.Y. Byun, W.B. Shim, S.U. Kim, M.G. Kim, High-sensitivity detection of ATP using a localized surface plasmon resonance (LSPR) sensor and split aptamers, Biosens. Bioelectron. 73 (2015) 26–31.
[31] L. Xie, X. Yan, Y. Du, An aptamer based wall-less LSPR array chip for label-free and high throughput detection of biomolecules, Biosens. Bioelectron. 53 (2014) 58–64.
[32] W.D. Pu, L. Zhang, C.Z. Huang, Graphene oxide as a nano-platform for ATP detection based on aptamer chemistry, Anal. Methods 4 (2012) 1662–1666.
[33] Y. Wei, Y. Chen, H. Li, S. Shuang, C. Dong, G. Wang, An exonuclease I-based label free fluorometric aptasensor for adenosine triphosphate (ATP) detection with a wide concentration range, Biosens. Bioelectron. 63 (2015) 311–316.
[34] K. Ma, H. Wang, H. Li, S. Wang, X. Li, B. Xu, W. Tian, A label-free aptasensor for turn-on fluorescent detection of ATP based on AIE-active probe and water-soluble carbon nanotubes, Sensor. Actuator. B Chem. 230 (2016) 556–558.
[35] J. Chen, Y. Liu, X. Ji, Z. He, Target-protecting dumbbell molecular probe against exonucleases digestion for sensitive detection of ATP and streptavidin, Biosens. Bioelectron. 83 (2016) 221–228.
[36] M. Zayats, Y. Huang, R. Gill, C. Ma, I. Willner, Label-free and reagentless aptamerbased sensors for small molecules, J. Am. Chem. Soc. 128 (2006) 13666–13667.